Journal of Power Sources 195 (2010) 5422–5425

Contents lists available at ScienceDirect

Journal of Power Sources

journal homepage: www.elsevier.com/locate/jpowsour

Short communication

Tungsten oxide bilayer electrodes for photoelectrochemical cells

Sung Jong Yoo[a], Seong Uk Yun[b], Yung-Eun Sung[b,*,1], Kwang-Soon Ahn[c,**,1]

[a] Fuel Cell Center, Korea Institute of Science and Technology (KIST), Seoul 136-791, Republic of Korea
[b] School of Chemical and Biological Engineering, Seoul National University, Seoul 151-742, Republic of Korea
[c] School of Display and Chemical Engineering, Yeungnam University, Gyeongbuk 712-749, Republic of Korea

ARTICLE INFO

Article history:
Received 13 January 2010
Received in revised form 18 February 2010
Accepted 3 March 2010
Available online 15 March 2010

Keywords:
Tungsten oxide
Bilayer
Photoelectrochemical cell
Electrochemical reaction sites
Electrical pathways

ABSTRACT

WO_3 bilayer electrodes composed of WO_3 top and bottom layers are designed for photoelectrochemical cells (PECs). The bottom layers are sputter-deposited at a high temperature (773 K) that leads to large grains and suitable electrical pathways for carrier collection. The top layer is deposited at a low temperature (573 K) and consists of small grains, which give rise to large electrochemical reaction sites. The bilayer electrodes give a significant enhancement in PEC performance compared with WO_3 monolayer electrodes deposited at 573 or 773 K, because of a combination of favourable effects.

1. Introduction

Photoelectrochemical cell (PEC) systems are a promising means for producing H_2 gas in an aqueous solution using solar energy [1–3]. The photoelectrochemical properties of a number of metal oxides, *e.g.*, TiO_2, WO_3, ZnO, Fe_2O_3, have been studied, and PEC systems based on TiO_2 have been extensively investigated [1,2,4–7]. TiO_2, however, is only photosensitive in the UV (ultra violet) light region because of its wide energy band-gap (3.2 eV). WO_3 has also been extensively studied in many technological areas, such as electrochromism [8–10], photocatalysis [11] and gas sensors [12], because of its nontoxic, stable, and inherent n-type semiconductor properties. WO_3 is one of a few inexpensive semiconductors that is resistant against photocorrosion in an acidic aqueous solution, and the energy band-gap of crystalline WO_3 is approximately 2.7 eV [8]. These properties suggest that WO_3 can be used as a promising alternative to TiO_2 in PECs, and has exhibited promising utilities in PEC systems [13–15].

Recently, WO_3/TiO_2 bilayered electrodes have been designed for effective charge separation in order to extend the lifetime of the electron–hole pairs and improve the photocatalytic activity [16,17]. The crystal phase of WO_3 plays an important role in the photocatalytic performance because the position of the conduction band of the semiconductor combined with TiO_2 must be similar to that of TiO_2 in order to prevent the formation of a Schottky energy barrier [7], which interferes with carrier transport. The level of the conduction band of crystalline WO_3 is below the crystalline TiO_2 film. Therefore, the bilayered TiO_2/WO_3 system contains amorphous WO_3 because its conduction band level is closer to anatase TiO_2 [16,17]. Amorphous WO_3, however, has some drawbacks. First, it has a wide band-gap energy (~3.4 eV) because of the quantum confinement effect in semiconductor clusters [8], which cannot absorb the long wavelength region in sunlight. Second, amorphous WO_3 contains a number of defect sites that lead to an increased bulk recombination rate because of inferior carrier transport [16]. Therefore, the amorphous phase is not desirable for PECs.

The photoelectrochemical responses are also affected by the electrochemical reaction sites, which can be increased by increasing the surface area (or decreasing the grain sizes) [18]. Crystalline WO_3 provides a superior electrical pathway for carrier collection and has a lower band-gap energy (~2.7 eV) compared with amorphous WO_3. By contrast, the number of electrochemical reaction sites is lower in the crystalline film because the large grains lead to an inferior PEC performance [16,19]. Therefore, approaches to improve all of the factors, such as the number of electrochemical reaction sites, the carrier transport and the optical band-gap, must be developed.

In this work, WO_3 bilayer structures consisting of bottom and top WO_3 layers are developed for PECs. The bottom layer is fabricated through sputter-deposition of WO_3 at 773 K, followed by a second sputter-deposition at 573 K for the top layer. The WO_3

* Corresponding author. Tel.: +82 2 880 1889; fax: +82 2 880 1604.
** Corresponding author. Tel.: +82 53 810 2524; fax: +82 53 810 4631.
E-mail addresses: ysung@snu.ac.kr (Y.-E. Sung), kstheory@ynu.ac.kr (K.-S. Ahn).
[1] Both these authors contributed equally to this work as the corresponding authors.

0378-7753/$ – see front matter © 2010 Elsevier B.V. All rights reserved.
doi:10.1016/j.jpowsour.2010.03.033

bilayer electrodes provided much better PEC performance than WO_3 monolayer electrodes deposited at 573 and 773 K because of the combined effect of the large number of electrochemical reaction sites and good electrical pathways.

2. Experimental

2.1. Preparation of WO_3 bilayer films

The WO_3 bilayer films were deposited on heated substrates using a reactive RF (radiofrequency) magnetron sputtering system. Transparent conducting oxides coated with fluorine-doped tin oxide (FTO, 8 Ω sq^{-1}) were used as the substrates. WO_3 served as the target material, and the distance between the target and the substrate was about 10 cm. The base pressure was below 6.67×10^{-4} Pa, and the working pressure was 1.33 Pa for all of the films. A pre-sputtering process was performed for 60 min to eliminate any contaminants in the target. The bottom WO_3 layers were sputter-deposited at 150 W and 773 K in ambient Ar:O_2 = 1:1, and then the substrate temperature was cooled to 573 K. The top layers were deposited on the bottom layers at 573 K and the same deposition rate (5 nm min^{-1}). The thicknesses of all of the bilayer films were set at 2 μm, and the thickness of the bottom layer varied from 0.7 to 1.3 μm. For comparison, 2 μm-thick WO_3 monolayer films were sputter-deposited at 573 and 773 K.

2.2. Structural and electrochemical characterization

The structure and crystallinity were characterized by means of X-ray diffraction (XRD). The surface morphology was examined using field-emission scanning electron microscopy (FE-SEM) to compare the grain sizes of the different films. Photoelectrochemical measurements were performed using a three-electrode cell with a flat quartz glass window to facilitate light illumination on the photoelectrode surface [19–21]. Sputter-deposited WO_3 films were used as working electrodes and had active surface area of about 0.6 cm^2. A Pt sheet (area: 10 cm^2) and an Ag|AgCl electrode (with saturated KCl) were used as the counter and reference electrodes, respectively, with a 1 M H_2SO_4 aqueous solution as the electrolyte. A xenon lamp (150 W) was used as the light source with a light intensity of 1×10^{-1} W cm^{-2}, which was measured with a photodiode power meter. The PEC responses were measured under chopped light on/off illumination using a potential sweep from 0.2 to 1.8 V (scan rate: 5×10^{-3} V s^{-1}).

3. Results and discussion

X-ray diffraction curves were measured for the FTO substrate and the 573 K- and 773 K-WO_3 films in order to confirm whether the films are crystalline or amorphous. The curves are shown in Fig. 1. Each of the WO_3 films exhibit a monoclinic, polycrystalline structure with a main peak at 24.4° that corresponds to the (2 0 0) plane. The crystallite size of the 773 K-WO_3 layer (21 nm) is similar to that of the 573 K-WO_3 layer (24 nm). Both films have similar optical band gaps in the range of 2.7–2.74 eV (not shown here), which correspond well to the optical band-gap (~2.7 eV) for crystalline WO_3.

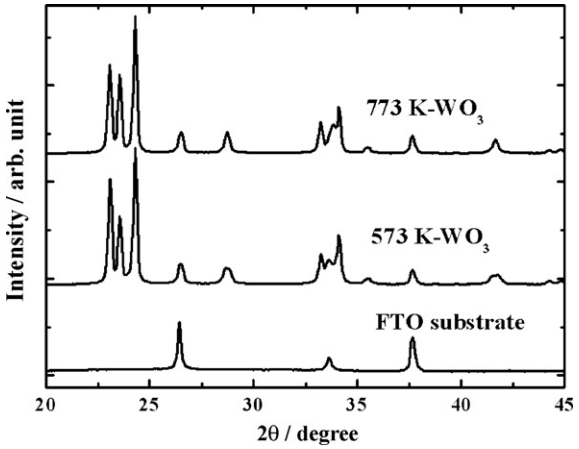

Fig. 1. X-ray diffraction patterns for 573 K- and 773 K-WO_3 monolayer films and FTO substrate.

Previous reports [22–24] have shown that the crystallite size is the coherent diffraction domain in the film, and the grain is composed of the crystallites. Fig. 2(a) and (b) shows FE-SEM images of the surface morphology of the 573 K- and 773 K-WO_3 films, respectively. In Fig. 1, the grains in the films are clearly much larger than the crystallites. The 573 K-WO_3 film is composed of grains that range in size from 300 to 540 nm but the 773 K-WO_3 film has much larger grain sizes, i.e. from 630 to 820 nm. Therefore, despite the similar crystallite sizes of the two films, the 573 K- and 773 K-WO_3 films have large differences in grain size.

Fig. 3 shows the current–voltage curves of the WO_3 monolayers and the bilayer (1.3 μm top layer and 0.7 μm bottom layer) for a potential range from −0.3 to 1 V in the dark. All of the samples exhibit typical electrochromic behaviour for WO_3 films at potentials below 0.2 V because of proton intercalation/deintercalation [8,25]. The electrochromic current density of the 573 K-WO_3 film is higher than that of the 773 K-WO_3 film. Electrochromic reactions occur mainly at the interface between the electrochromic materials and the electrolyte [8]. Therefore, the small grains of the 573 K-WO_3 film in Fig. 2 provide a larger number of electrochemical reaction sites, which gives rise to the higher electrochromic current density.

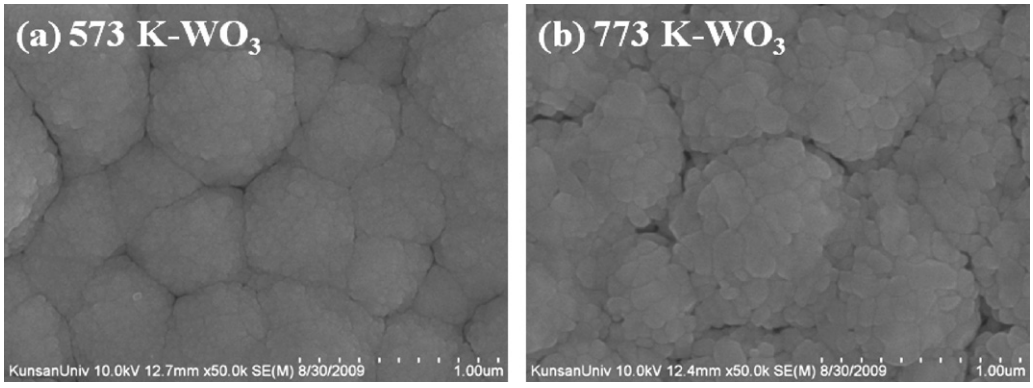

Fig. 2. FE-SEM images of (a) 573 K- and (b) 773 K-WO_3 monolayer films.

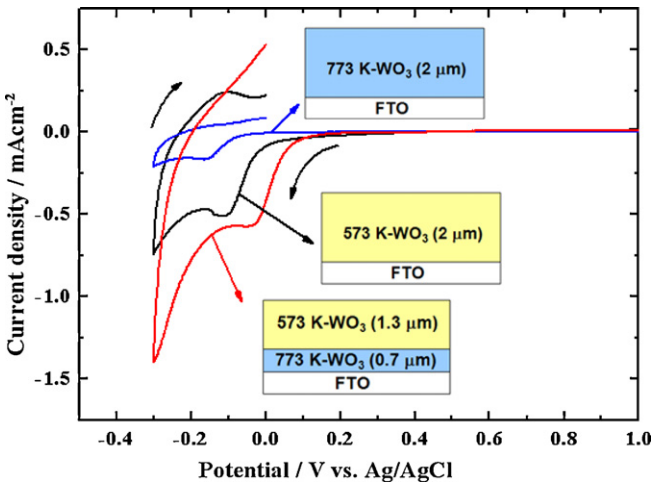

Fig. 3. Electrochromic current–voltage curves for 573 K- and 773 K-WO_3 monolayer films and bilayer film, where 573 K-top and 773 K-bottom layers have a thickness of 1.3 and 0.7 μm, respectively.

The bilayer film exhibits a significantly enhanced electrochromic current density compared with the 573 K-WO_3 monolayer. The electrochemical reaction is influenced by carrier transport properties as well as by electrochemical reaction sites [18–20]. The large grains in the film enhance the carrier transport properties because electrical isolation or boundary scattering is decreased, whereas the number of electrochemical reaction sites is also decreased. The bilayer electrode is composed of 573 K-top and 773 K-bottom layers because the 573 K-top layer provides a larger number electrochemical reaction sites, and the 773 K-bottom layer provides suitable electrical pathways for carrier collection. The significantly enhanced electrochromic current density of the bilayer structure is most likely caused by the combined effect of the larger number of electrochemical reaction sites and the good carrier transport [26,27].

Fig. 4(a)–(c) show photocurrent–voltage curves for 573 K- and 773 K-WO_3 films and the WO_3 bilayer film, respectively, measured under chopped light on/off illumination. The inset of Fig. 4(b) gives the current–voltage curve for the 773 K-WO_3 film over a wide potential range from −0.3 to 1.5 V in the dark (upper curve) and under chopped light on/off illumination (lower curve). The data show that a photoelectrochemical response appears at potentials above 0.3 V. The repeated proton intercalation/deintercalation in the electrochromic region below 0.2 V causes structural transformation and affects the photoresponse [28]. Therefore, only freshly prepared samples were used for the photoresponse experiments. The thickness of the bottom layer of the 2 μm-thick bilayer films varies from 0.7 to 1.3 μm, and the PEC measurements were performed for the films (not shown here). The photocurrents for all of the samples were plotted at 1.6 V to compare the PEC responses [Fig. 4(d)]. The photocurrent of the 573 K-WO_3 film is better than that of the 773 K-WO_3, despite their similar optical band-gaps, because of the larger number of electrochemical reaction sites created by the small grains in the 573 K-WO_3 film. As seen in Fig. 3, the electrochromic response of the bilayer film is much higher than that of the 573 K-WO_3 film because of the large number of electro-

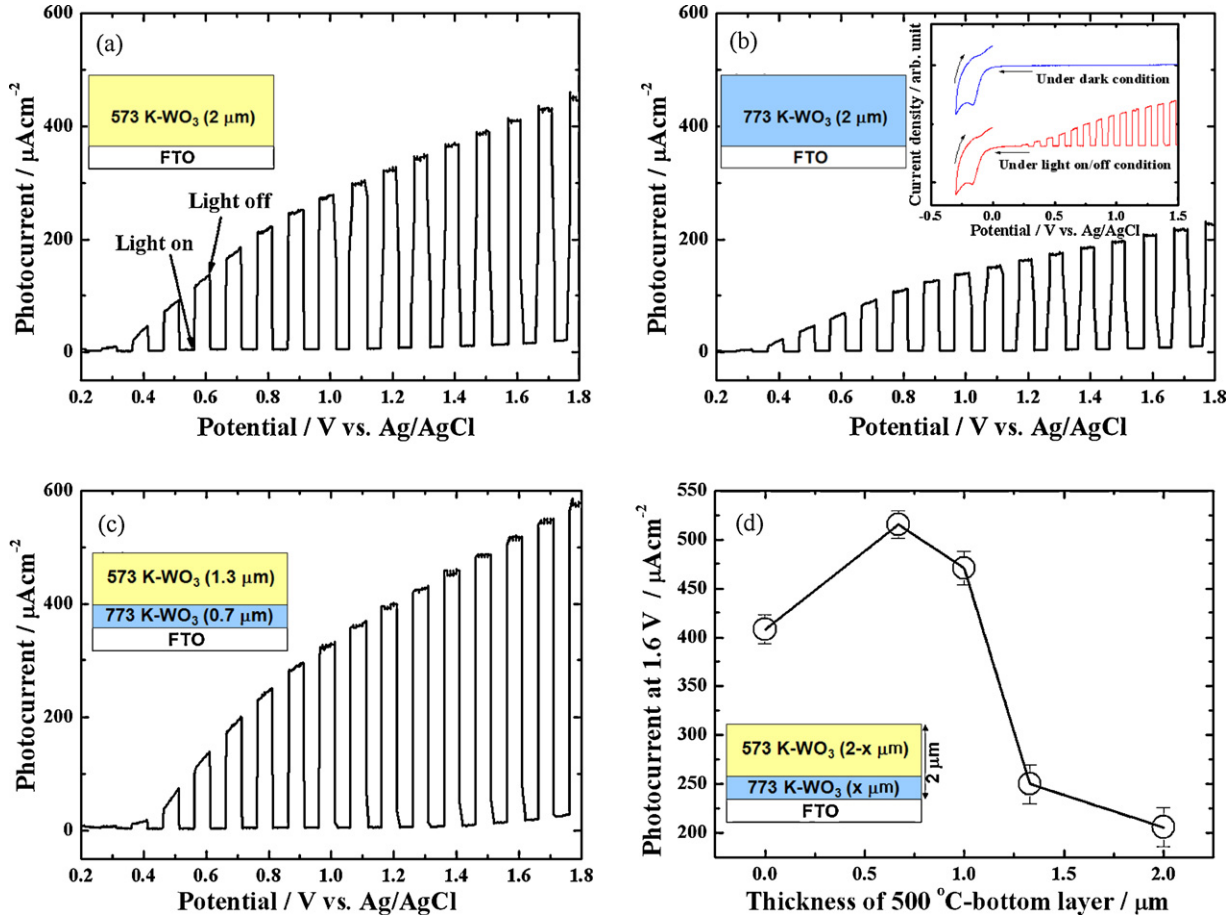

Fig. 4. Photocurrent–voltage curves for (a) 573 K- and (b) 773 K-WO_3 monolayer films and (c) bilayer film (consisting of 1.3 μm-top and 0.7 μm-bottom layers) measured under chopped light on/off illumination. (d) Photocurrents at 1.6 V for monolayer films and bilayer films with different thickness ratios of bottom and top layers. Inset in (b) gives current–voltage curves for 773 K-WO_3 film over wide potential range (−0.3 to 1.5 V) in dark (upper curve) and under chopped light illumination (lower curve).

chemical reaction sites and the good carrier transport properties that are provided by the small grains of the 573 K-top layer and the large grains of the 773 K-bottom layer, respectively. The information in Fig. 4(d) clearly shows that bilayer electrodes with bottom layers of thickness less than 1 μm exhibit significantly enhanced PEC responses compared with the 573 K-WO_3 film. The bilayer electrode consisting of a thin (0.7 μm) 573 K-top layer on a thick (1.3 μm) 773 K-bottom layer gives a better PEC response than the 773 K-WO_3 film. Therefore, bilayer structures provide not only a large number of electrochemical reaction sites but also suitable electrical pathways that result in significantly improved PEC performance. Comparative PEC performance tests were repeated for many experimental runs to ensure that the results were reproducible.

4. Conclusions

WO_3 bilayer electrodes composed of a 573 K-top layer and a 773 K-bottom layer have been deposited using a reactive RF magnetron sputtering system on heated substrates. The 573 K- and 773 K-deposited films have similar crystallite size and optical band-gaps but there is a large difference in the grain size. The 573 K-top layer of the bilayer film provides a large number of electrochemical reaction sites because of the small grains. Carrier transport to the FTO substrates is enhanced by the large grains in the 773 K-bottom layer. The combination of these favourable effects results in significantly increased PEC performance from bilayer electrodes compared with 573 K- and 773 K-WO_3 monolayer films. These findings are expected to provide valuable insight into the development of multi-layered electrodes for PEC applications including photocatalysts, electrochromic devices, and batteries.

Acknowledgements

This work is supported by the Ministry of Education, Science & Tehnology (MEST) and the National Research Foundation of Korea (NRF) under a Project “Human Resource Development Center for Economic Region Leading Industry”.

References

[1] A. Fujishima, K. Honda, Nature 238 (1972) 37.
[2] R. Asahi, T. Morikawa, T. Ohwaki, K. Aoki, Y. Taga, Science 293 (2001) 269.
[3] O. Khaselev, J.A. Turner, Science 280 (1998) 425.
[4] V.M. Aroutiounian, V.M. Arakelyan, G.E. Shahnazaryan, Solar Energy 78 (2005) 581.
[5] A. Ghicov, H. Tsuchiya, J.M. Macak, P. Schmuki, Phys. Stat. Sol. (a) 203 (2006) R28.
[6] G.K. Mor, K. Shankar, M. Paulose, O.K. Varghese, C.A. Grimes, Nano Lett. 5 (2005) 191.
[7] B. O'Regan, M. Grätzel, Nature 353 (1991) 737.
[8] C.G. Granqvist (Ed.), Handbook of Inorganic Electrochromic Materials, Elsevier Science, Amsterdam, 1995.
[9] S.J. Yoo, Y.H. Jung, H.G. Choi, D.K. Kim, J.W. Lim, Y.-E. Sung, Appl. Phys. Lett. 70 (2007) 173126–173131.
[10] Y. Wang, N. Herron, J. Chem. Phys. 95 (1991) 525.
[11] H. Bosch, F. Janssen, Catal. Today 2 (1988) 424.
[12] W.H. Tao, C.H. Tsai, Sens. Actuators B: Chem. 81 (2002) 237.
[13] E.L. Miller, D. Paluselli, B. Marsen, R.E. Rocheleau, Sol. Energy Mater. Sol. Cell 88 (2005) 131.
[14] E.L. Miller, B. Marsen, D. Paluselli, R. Rocheleau, Electrochem. Solid State Lett. 8 (2005) A247.
[15] K. Sivula, F.L. Formal, M. Grätzel, Chem. Mater. 21 (2009) 2862.
[16] S. Higashimoto, Y. Ushiroda, M. Azuma, Top. Catal. 47 (2008) 148.
[17] W. Smith, Y. Zhao, J. Phys. Chem. C 112 (2008) 19635.
[18] C.M. López, K.-S. Choi, Chem. Commun. 26 (2005) 3328.
[19] K.-S. Ahn, S. Shet, T. Deutsch, C.-S. Jiang, Y. Yan, M. Al-Jassim, J. Turner, J. Power Sources 176 (2008) 387.
[20] K.-S. Ahn, Y. Yan, S. Shet, K. Jones, T. Deutsch, J. Turner, M. Al-Jassim, Appl. Phys. Lett. 93 (2008) 163117.
[21] K.-S. Ahn, Y. Yan, M.-S. Kang, J.-Y. Kim, S. Shet, H. Wang, J. Turner, M. Al-Jassim, Appl. Phys. Lett. 95 (2009) 022116.
[22] J.R. Ares, A. Pascual, I.J. Ferrer, C. Sánchez, Thin Solid Films 480–481 (2005) 477.
[23] E. Leite, M.I.B. Bernardi, E. Longo, J.A. Varela, C.A. Paskocimas, Thin Solid Films 449 (2004) 67.
[24] M.L. Lavcevic, A. Turkovic, Scr. Mater. 46 (2002) 501.
[25] S.H. Lee, R. Deshpande, P.A. Parilla, K.M. Jones, B. To, A.H. Mahan, A.C. Dillon, Adv. Mater. 18 (2006) 763.
[26] C. Cantalini, H.T. Sun, M. Faccio, M. Pelino, S. Santucci, L. Lozzi, M. Passacantando, Sens. Actuators B-Chem. 31 (1996) 81.
[27] A. Enesca, A. Duta, L. Isac, S. Manolache, J. Schoonman, J. Phys.: Conf. Ser. 61 (2007) 472.
[28] B. Reichman, A.J. Bard, J. Electrochem. Soc. 126 (1979) 2133.